Protein Response to External Electric Fields: Relaxation, Hysteresis, and Echo

Dong Xu,† James Christopher Phillips, and Klaus Schulten*

Department of Physics and Beckman Institute, University of Illinois at Urbana−Champaign, Urbana, Illinois 61801

Received: January 4, 1996[⊗]

Dipole moments induced in proteins by external electric fields are studied by molecular dynamics simulations and described in terms of analytical models based on ensembles of Langevin oscillators and Fokker−Planck equations. We investigate through simulations of the protein bovine pancreatic trypsin inhibitor (BPTI) (1) the distribution $p(M)$ of dipole moments as well as the dipole moment autocorrelation function $C_{M,M}(t)$ at thermal equilibrium, (2) the dielectric constant ϵ, (3) the dipole moment $\Delta M(t)$ induced by cyclic (piecewise linear or sinusoidally periodic in time) spatially homogeneous fields, demonstrating significant hysteresis behavior, and (4) the dipolar response to a constant homogeneous field applied for about a picosecond. Through a comparison between an analytical model and simulations, we show that the dipolar response (4) can be described by a relaxation characterized by $C_{M,M}(t)$ in addition to a significant pulse-shaped component, termed the dipole echo. The dipole echo arises from a memory effect of transient increases or decreases of protein vibrational frequencies induced by an external field. The hysteresis behavior (3) under a weak external field is related to the equilibrium properties $p(M)$, $C_{M,M}(t)$, and ϵ; however, discrete structural transitions induced by a strong field also contribute to hysteresis, as demonstrated in a model evoking stochastic motion in a periodically driven bistable potential. In the case of electric fields arising through charge displacements in proteins, e.g., through electronic excitation or photoinduced electron transfer, concomitant dipolar responses in real proteins should resemble those reported here and should be observable by means of sub-picosecond spectroscopy.

I. Introduction

The dielectric properties of proteins are significantly different from those of solvents.[1−3] Unlike solvents, proteins have well-defined structures; charged and polar groups in proteins can move little in response to an external electric field. Furthermore, dipolar relaxation, associated with nuclear degrees of freedom, varies significantly between different regions of a protein.[4,5] Molecular dynamics simulations provide a useful tool to link dielectric properties and dipolar relaxation to the structure and dynamics of proteins quantitatively.

There is no doubt that dielectric properties of globular proteins in solvent are essential for their function.[6,7] The particular effect of solvents in this regard has been addressed in a number of molecular dynamics studies.[8−10] However, because of the high dielectric constant of bulk water and since protein solutions cannot be made very concentrated, it is very difficult to measure dielectric properties of the interior of a solvated protein experimentally. To overcome these difficulties, extensive measurements have been made on dry powders and hydrated powders of proteins.[11−14] It appears then desirable to model the dielectric behavior of proteins without the presence of solvent. The studies on dry proteins can also shed some light on transmembrane proteins, for which solvents are not expected to play a major role. Accordingly, we investigate in this paper equilibrium and non-equilibrium dielectric properties of a protein in vacuum. We choose for our study the protein bovine pancreatic trypsin inhibitor (BPTI).[15]

The dielectric properties of a protein, together with particular protein configurations, can accelerate chemical reactions which otherwise proceed slowly or not at all.[2,6,16,17] One of the key characteristics in this regard is the dielectric response of a protein to charge shifts connected with photobiological reactions, e.g., electron transfer,[18−24] proton transfer,[8] or electronic excitation.[25,26] In the last case, an electronically excited state is often populated for a time of picoseconds or less and brings about a brief change of the dipole moment of the electronically excited group to which the protein matrix exhibits a dielectric response.[27] To develop a better understanding of the dynamics of photobiological reactions, one should study the response of proteins to an electric field pulse which is switched on at time $t = 0$ and is switched off at time $t = \tau$.

Consecutive perturbations in proteins have been studied in the context of temperature quench echoes[28,29] and velocity reassignment echoes.[30] These echoes are generated by imposing two perturbations on the atomic velocities of a protein, one at time $t = 0$ and one at time $t = \tau$, such that a coherent excitation of protein modes is generated which induces an echo at a certain time after the second perturbation, e.g., at time $t = 3\tau/2$ [30] or at time $t = 2\tau$.[28,29] In the present study, we will employ concepts similar to those used in refs 29 and 30 and investigate dipolar responses to electric field pulses in terms of a model representing a protein's degrees of freedom as an ensemble of Langevin oscillators.

The application of time-dependent fields induces dissipative processes in proteins which surface, for example, through hysteretic behavior. We demonstrate such behavior through simulation and compare the results to a simple analytical description which holds in linear response theory as well as to a model involving metastable protein conformations and governed by a Smoluchowski equation with a periodic bistable potential.

In section II of this paper, we discuss briefly the molecular dynamics simulation methods employed in our study. In section

* To whom correspondence should be addressed. E-mail: kschulte@ks.uiuc.edu.

† Current address: Laboratory of Mathematical Biology, SAIC, NCI-FCRDC, P.O. Box B, Building 469, Frederick, MD 21702.

⊗ Abstract published in *Advance ACS Abstracts,* June 15, 1996.

S0022-3654(96)00076-7 CCC: $12.00

III we present results of the simulations of proteins showing dipole changes subjected to continuous electric fields, to cyclic fields, and to field pulses. In section IV, we provide analytical descriptions, together with numerical experiments, to analyze in detail the dipolar response of BPTI to a field pulse as well as hysteresis in the presence of periodic fields. In section V, we summarize and discuss our results.

II. Methods

All simulations described in this paper were carried out for the protein BPTI in vacuum, starting from the 1.5 Å resolution X-ray structure[15] and using the molecular dynamics package MD/PMD[31] together with a fast multipole algorithm for the evaluation of Coulomb forces.[32] The CHARMm all-atom potential energy function (parmallh3x.pro) and CHARMm partial charge assignment (topallh6x.pro) were used.[33] The dielectric constant was $\epsilon = 1$, and the time step in our simulations was chosen as 1 fs. Coulomb and van der Waals interactions were calculated exactly; i.e., no distance cutoff for nonbonded interactions was used. Explicit hydrogen bonding terms in the energy function were not employed. Equilibrated structures at various temperatures T_0 were achieved through coupling to a heat bath by rescaling velocities according to

$$v_i^{\text{new}} = v_i^{\text{old}}[1 - \lambda + \lambda T_0/T_i]^{1/2} \tag{1}$$

Here T_i is the temperature at the ith integration step evaluated through the kinetic energy, i.e., using

$$T_i = \frac{2}{3k_B N}\sum_{\alpha=1}^{N}\frac{1}{2}m_\alpha \vec{v}_{\alpha,i}{}^2 \tag{2}$$

A value $\lambda = 0.01$ had been chosen for the coupling strength in (1). Once structures had been equilibrated at a given temperature, all simulations were carried out without applying any coupling to a heat bath; in particular, during applications of external fields, couplings to a heat bath were not employed.

The total electric dipole moment along the $\hat{x}$ direction at time t was calculated through

$$M(t) = \sum_{\alpha=1}^{N}(q_\alpha - q_0)x_\alpha(t), \quad q_0 = \frac{1}{N}\sum_{\alpha=1}^{N} q_\alpha \tag{3}$$

where the x-coordinate had been chosen in the direction of the applied field; q_α is the partial charge on atom α, x_α is the x-coordinate of atom α, and N is the number of atoms; i.e., $N = 898$ in BPTI. It can be readily shown that subtraction of the monopole contribution q_0 renders (3) independent of the choice of the coordinate origin. For the sake of simplicity, we do not consider overall translations and rotations of the protein induced by the external field. Accordingly, the center of mass movement and the overall rotation of the protein were removed at every integration step. We exclude the study of tensorial effects, i.e., a dipolar response in directions other than that of the applied field.

The autocorrelation function of the dipole moment $M(t)$, defined in (3), is

$$C_{M,M}(t) = \frac{\langle (M(t) - \langle M\rangle)(M(0) - \langle M\rangle)\rangle}{\langle (M(0) - \langle M\rangle)^2\rangle} \tag{4}$$

where $\langle ...\rangle$ denotes the equilibrium average, which is calculated as a time average over a certain time period of dynamics of the equilibrated system. Accordingly, $C_{M,M}(t)$ is determined by applying the formula

$$C_{M,M}(i\Delta t) = \frac{1}{N_t\langle \tilde{M}^2\rangle}\sum_{j=1}^{N_t}\tilde{M}(i\Delta t + j\Delta t)\,\tilde{M}(j\Delta t) \tag{5}$$

where $\tilde{M} = M - \langle M\rangle$ and where Δt is the time step of integration, i.e., 1 fs in the present case. To determine $C_{M,M}(t)$ for the time interval $0 < t < L\Delta t$ from a trajectory with a total number of integration steps K, one chooses N_t in (5) equal to $K - L$. The position autocorrelation function $C_{x,x}(t)$, defined in (9) below, is calculated in an analogous way.

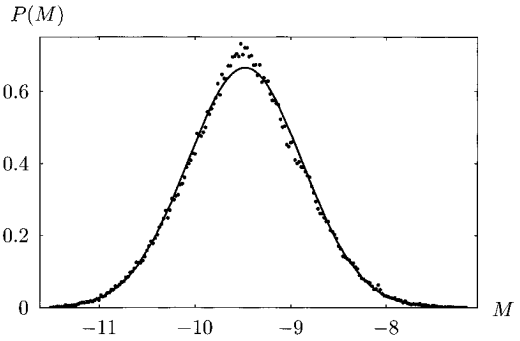

Figure 1. Distribution of the electric dipole moment due to thermal fluctuations at temperature 102.2 K and a Gaussian distribution with matching mean and variance.

III. Results

In this section we present the results of molecular dynamics simulations on the protein BTPI for the dipole moment equilibrium autocorrelation function $C_{M,M}(t)$, the evolution of the root mean square deviation (RMSD) under electric fields, the position autocorrelation function $C_{x,x}(t)$ with and without an external field, the electric polarization together with the dielectric constant, the dipole moment induced by cyclic (sinusoidally or piecewise linear periodic in time) homogeneous fields, and the dipole moment response to a constant field applied for about a picosecond.

A. Dipole Moment Distribution and Autocorrelation Function. The distribution and autocorrelation function $C_{M,M}(t)$ of the dipole moment, the latter defined in (4), have been determined from a 100 ps trajectory at $T = 102$ K. The distribution, shown in Figure 1, is nearly Gaussian. The average dipole moment is

$$M_0 = -9.41 \text{ e Å} \tag{6}$$

with a standard deviation

$$\sigma_M = 0.60 \text{ e Å} \tag{7}$$

Figure 2 presents the autocorrelation function. One can see that $C_{M,M}(t)$, after an initial decay, exhibits damped oscillations. The short time decay of $C_{M,M}(t)$ can be matched to a single exponential

$$C_{M,M}(t) \approx \mathrm{e}^{-t/\tau_0}; \quad \tau_0 = 185 \text{ fs} \tag{8}$$

The behavior of $C_{M,M}(t)$, including the time scale τ_0, is similar to that reported for proteins without solvent by King et al.[8]

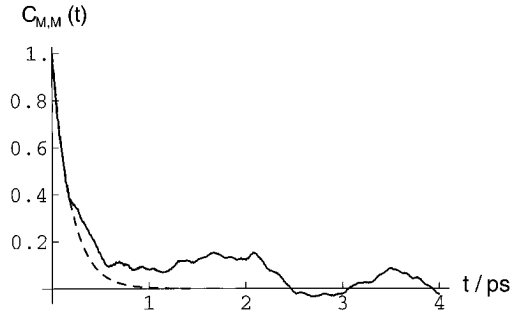

Figure 2. Autocorrelation function of the dipole moment $M(t)$ as defined by (4), at temperature 102.2 K (solid line). The broken line represents the single exponential decay given by (8).

B. Root Mean Square Deviation. We seek to determine now the structural change induced by application of an external electric field. For this purpose, we monitored the RMSD of the protein structure versus time, the results being presented in Figure 3. Two closely related simulations have been carried out; both started from the same initial coordinates and velocities at $T_0 = 100$ K. After 10 ps dynamics at a time defined as $t = 0$, one simulation continued without an applied field, while the protein in the second simulation experienced a static homogeneous field of strength 1×10^8 V/m. The RMSD relative to the structure at $t = 0$, when the field had been switched on for one of the simulations, are shown in Figure 3. The RMSD values stay closely together for the two simulations until about $t = 0.2$ ps and deviate thereafter from each other, however, remaining in close range. The results demonstrate that a field of strength 10^8 V/m does not alter the overall structure of BPTI significantly.

To test in how far a stronger field may alter this behavior, we carried out two analogous simulations, albeit for a field of strength 2×10^9 V/m applied for 1, 2, and 3 ps durations and applied as a static field. Figure 4 demonstrates that such a strong field changes the structure of BPTI significantly when applied for 2 ps or longer and that the structural deformation does not relax quickly after the field has been turned off. In fact, the RMSD after a 1 ps field pulse remains in the same range as that without an applied field; i.e., no significant change of overall protein structure occurs in this case. However, if the field is applied for 2 or 3 ps, the RMSD differs substantially from the case without any external field, even after the field is turned off. This implies that BPTI undergoes a structural change in a stronger field which does not revert on the time scale shown (20 ps). When a field of 2×10^9 V/m is applied for 150 ps, the RMSD values stabilize within about 5 ps at a value of about 2 Å, as shown in Figure 4. Accordingly, one does not need to worry about a possible unfolding of BPTI under the influence of a field as strong as 2×10^9 V/m, at least for a time span of a few tens of picoseconds.

The protein response is expected to depend on temperature. To investigate this dependence, we determined the RMSD of BPTI simulated in a field-free situation and in the presence of an external field at $T_0 = 300$ K, i.e., at a physiological temperature. The results are presented in Figure 5. The RMSD at 300 K is seen to stabilize more slowly than at 100 K, indicating that the protein at $T_0 = 300$ K explores more conformations than at 100 K. In fact, the RMSD values for electric fields of 2×10^9 V/m of duration 1, 2, and 3 ps, starting from 300 K, are closer to the converged field-free RMSD values than they are at 100 K. Hence, more conformational sampling is required for studies of dipolar responses at 300 K.

C. Position Autocorrelation Function. In order to demonstrate that individual atoms change their motion significantly

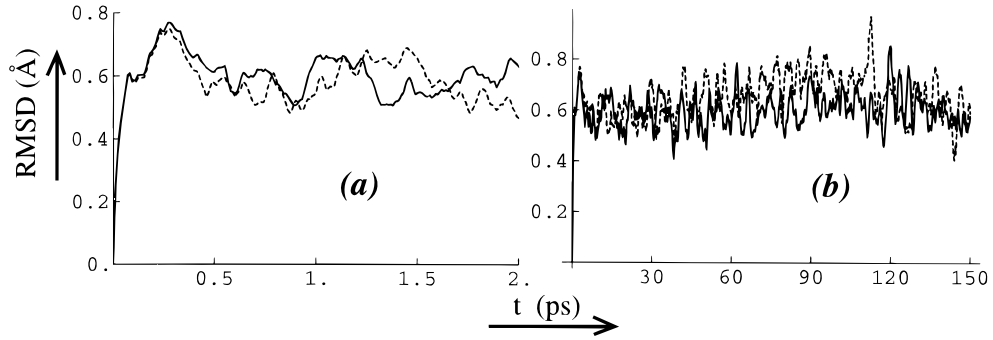

Figure 3. RMSD from the structure at $t = 0$ for a simulation without an external field (broken lines) and for a simulation with a static, homogeneous field of 1.00×10^8 V/m (solid lines). The two simulations started, at $t = 0$, from identical initial positions and velocities, the latter generated for $T_0 = 100$ K; (a) depicts the short time behavior of (b).

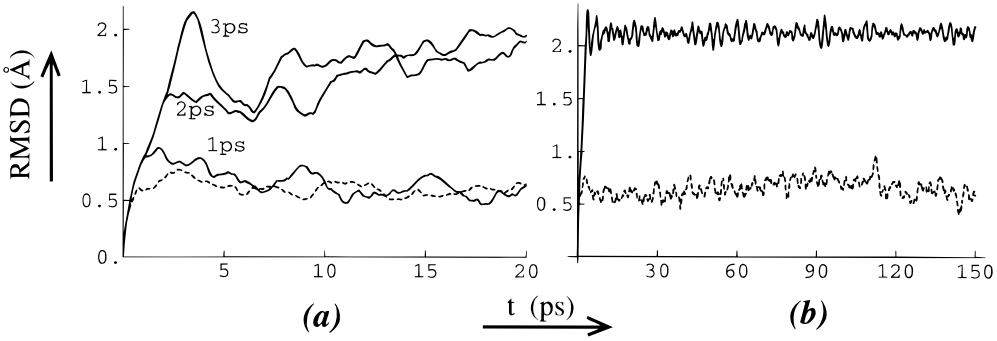

Figure 4. RMSD from the structure at $t = 0$ for a simulation without an external field (broken lines) and for a simulation with a homogeneous field of 2×10^9 V/m (solid lines). (a) shows the RMSD for a simulation under the influence of an electric field of duration 1, 2, and 3 ps, starting at $t = 0$. (b) shows the RMSD for a simulation with a static field. All the trajectories started from identical initial positions and velocities, the latter generated for $T_0 = 100$ K.

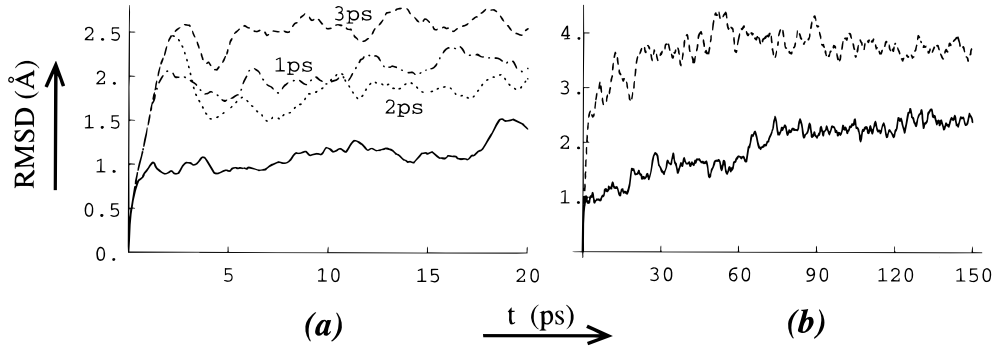

Figure 5. RMSD of BPTI at $T_0 = 300$ K. Solid lines are for a simulation without an external field; broken lines are for a simulation with a homogeneous field of 2×10^9 V/m, starting at $t = 0$. All trajectories started from identical initial positions and velocities at $t = 0$. (a) RMSD values for a simulation under the influence of an electric field of duration 1, 2, and 3 ps. (b) RMSD values for a simulation in a static field.

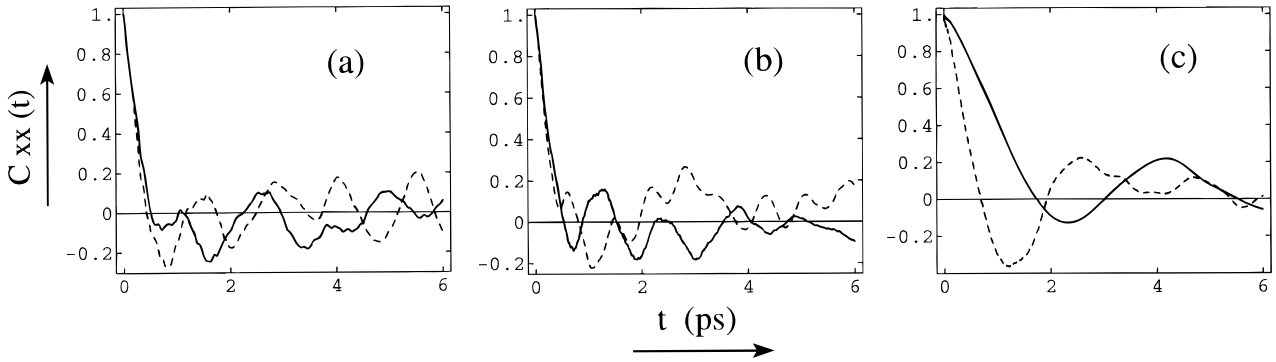

Figure 6. Autocorrelation function $C_{x,x}(t)$, defined by (9), (a) for the amide nitrogen of Arg-1, (b) for C^γ of Arg-17, and (c) for the hydrogen attached to C^α of Ile-18 without an external field (broken lines) and with a static field of strength 2.17×10^9 V/m (solid lines). $T_0 = 100$ K.

upon application of an external field, we determined the position autocorrelation function

$$C_{x,x}(t) = \frac{\langle (x(t) - \langle x \rangle)(x(0) - \langle x \rangle) \rangle}{\langle (x(0) - \langle x \rangle)^2 \rangle} \tag{9}$$

where x denotes the coordinate of a specific atom in the direction of the applied field. Figure 6 shows $C_{x,x}(t)$ for three atoms of BPTI without applied external field, and in a constant external electric field of magnitude 2.17×10^9 V/m. The chosen atoms represent exemplary atoms in a protein, namely, a backbone atom, a side chain atom, and an atom near a terminus. The average temperature of the 80 ps trajectory used to calculate the correlation function in the absence of a field was $T = 102.2$ K. To determine $C_{x,x}(t)$ in the presence of the electric field, we started from an equilibrated structure (without field) at $T = 100$ K; we then added the electric field without applying any coupling to a heat bath and equilibrated the system for 40 ps; the subsequent 80 ps simulation served to determine $C_{x,x}(t)$. The average temperature of the system during the 80 ps simulation in the external electric field was $T = 117.1$ K. One can see from Figure 6 that there is a significant difference in the correlation function $C_{x,x}(t)$ with the external field and without one. The difference is stronger in the case of the hydrogen attached to C^α of Ile-18, which is linked directly to the protein backbone in the core of the protein, than in the cases of an atom in a side group at the N-terminus (the amide nitrogen of Arg-1) and of a side chain atom (C^γ of Arg-17), both of which are near the surface of the protein.

D. Evaluation of the Dielectric Constant. The dielectric constant ϵ of a medium can be determined through application of a static electric field E and measurement of the electric susceptibility χ_e. The following well-known relationship applies

$$\epsilon = 1 + \chi_e \tag{10}$$

The susceptibility relates the strength of the applied field to the polarization P, defined as the electric dipole moment of the medium per unit volume

$$P = \epsilon_0 \chi_e E \tag{11}$$

Accordingly, the dielectric constant can be determined through

$$\epsilon = 1 + \frac{P}{\epsilon_0 E} \tag{12}$$

Conventionally, the polarization is determined through an ensemble average. One may employ, instead, a time average $\langle ... \rangle_t$ to calculate P based on a sufficiently long molecular dynamics simulation

$$P = \langle \Delta M \rangle_t / V \tag{13}$$

Here ΔM is the total dipole moment change induced by the external field, and V is the volume of the material. In the case of BPTI the volume measures 6758 Å^3 as calculated using the program MS[34,35] for the X-ray structure of BPTI.

To determine $\Delta M(t)$, we employed again two trajectories, both starting with identical coordinates and velocities selected from a Maxwell distribution at $T_0 = 100$ K. After 10 ps dynamics, one simulation continued without a field, while the other incorporated a static homogeneous field of 1×10^8 V/m. The difference $\Delta M(t)$ of the dipole moments of BPTI for the two trajectories exhibits significantly less fluctuation than encountered when independent simulations describing the field-off and field-on cases are compared. Figure 7 presents $\Delta M(t)$ evaluated accordingly. One can discern that $\Delta M(t)$ gradually reaches its equilibrium value, while the fluctuations become larger and larger. In the time range 10 ps $< t \leq$ 110 ps, $\langle \Delta M \rangle$ assumes a value of 0.606 e Å. Application of (12) and (13) yields then a

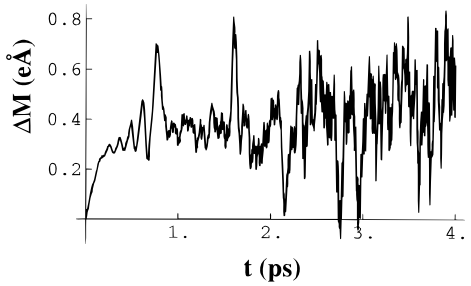

Figure 7. Dipole moment $\Delta M(t)$ induced in BPTI in the direction of an external field of 10^8 V/m. $\Delta M(t)$ measures the dipole moment relative to the dipole moment of field free BPTI described in a simulation with identical initial positions and velocities, the latter generated for $T_0 = 100$ K.

value of the dielectric constant

$$\epsilon = 2.62 \tag{14}$$

The above non-equilibrium molecular dynamics technique had been applied in a similar form to determine diffusion coefficients of small gas molecules in polymers from the mean-square displacement under a fictitious external field.[36]

One can evaluate the dielectric constant also from fluctuations of the total dipole moment, employing the relationship[37,38]

$$\epsilon = \frac{3 + 2\alpha}{3 - \alpha}; \quad \alpha = \frac{\sigma_M^{\,2}}{\epsilon_0 V k_B T} \tag{15}$$

where σ_M is the standard deviation of the dipole moment along the direction of the applied field. σ_M assumes a value 0.60 e Å in the present case [see also (7)], and, accordingly, one obtains the alternative value

$$\epsilon = 2.78 \tag{16}$$

for the dielectric constant, which is close to the value in (14). This agreement lends credence to the validity of the non-equilibrium dipolar properties simulated in our study.

E. Response to Cyclic Fields. Hysteresis effects have been generated in BPTI by periodically driving the system with a weak, sinusoidal, homogeneous electric field, as shown in Figure 8. Starting from a well-equilibrated protein in zero field at $T = 100$ K, we applied a time-dependent spatially homogeneous field $E(t)$ of the form

$$E(t) = E_0 \sin(\Omega t); \quad \Omega = 2\pi/t_p \tag{17}$$

for $E_0 = 1 \times 10^8$ V/m, i.e., for a relatively weak field. The initial 200 ps of dynamics allowed equilibration to the new state generated by the external field. This equilibration period was sufficient since 200 ps is much longer than the relaxation time $\tau_0 = 185$ fs as defined in (8). During the next 200 ps, we determined $\Delta M(t)$. The solid lines in Figure 8 show the dipole response averaged over many cycles, denoted by $\langle \Delta M(t) \rangle$, versus the quantity $E(t)/E_0 = \sin(\Omega t)$ for $t_p = 100$, 500, and 2000 fs. The traces of $\{E(t)/E_0, \langle \Delta M(t) \rangle\}$ circumscribe significant areas for all periods t_p chosen, indicating a hysteresis effect. If this effect were not present, the traces would be reduced to a single line. The broken lines in Figure 8 show the theoretical prediction based on a model derived below.

A larger hysteresis effect arises in BPTI under the influence of a strong cyclic electrical field, as illustrated in Figure 9. Starting from a well-equilibrated protein in zero field at $T = 100$ K, denoted as state a in Figure 9, we applied a time-dependent cyclic spatially homogeneous field. The field $E(t)$, during the initial time interval $0 \le t < t_0$, $t_0 = 5$ ps, was linearly increased from $E(0) = 0$ to $E_0 = 2.17 \times 10^9$ V/m; i.e., we applied the field $E(t) = E_0 t/t_0$ during the stated time period. The state of the protein at $t = 5$ ps is denoted as b in Figure 9. We then decreased the field linearly to $E_0 = -2.17 \times 10^9$ V/m during the time interval $t_0 \le t < 3t_0$; i.e., we applied the field $E(t) = E_0(2t_0 - t)/t_0$. The states of the protein at times $t = 2t_0 = 10$ ps and $t = 3t_0 = 15$ ps are denoted in Figure 9 by c and d, respectively. We then increased again the field to a value $E_0 = 2.17 \times 10^9$ V/m during the time interval $3t_0 \le t \le 5t_0$; i.e., we applied the field $E(t) = E_0(t - 4t_0)/t_0$. The states of the protein at times $t = 4t_0 = 20$ ps and $t = 5t_0 = 25$ ps are denoted in Figure 9 by e and f, respectively. During the application of the field we monitored the dipole moment change $\Delta M(t)$ relative to the dipole moment at $t = 0$. Since the period of 20 ps of the applied cyclic field is much longer than the relaxation time τ_0 as defined in (8), the protein can relax significantly in the presence of the applied field.

In Figure 9 we plotted, in the fashion of a hysteresis diagram, the values $(E(t), \Delta M(t))$ during the period $0 \le t \le 25$ ps. We indicate in the figure the states a−f of the protein. The portion $a \rightarrow b$ of the hysteresis diagram describes the initial polarization. Following this, a strong hysteresis effect develops. Figure 9 clearly shows that the $(E(t), \Delta M(t))$ loop during the process $b \rightarrow c \rightarrow d \rightarrow e \rightarrow f$ circumscribes a large area in E, ΔM space, indicating a significant hysteresis effect in the protein at the chosen temperature. The effect is conventionally attributed to an irreversible motion inside the system[39] and is studied further below. The strong hysteresis shown in Figure 9 corroborates the findings shown in Figure 4, namely, that structural changes induced by a field of strength 2×10^9 V/m do not relax during

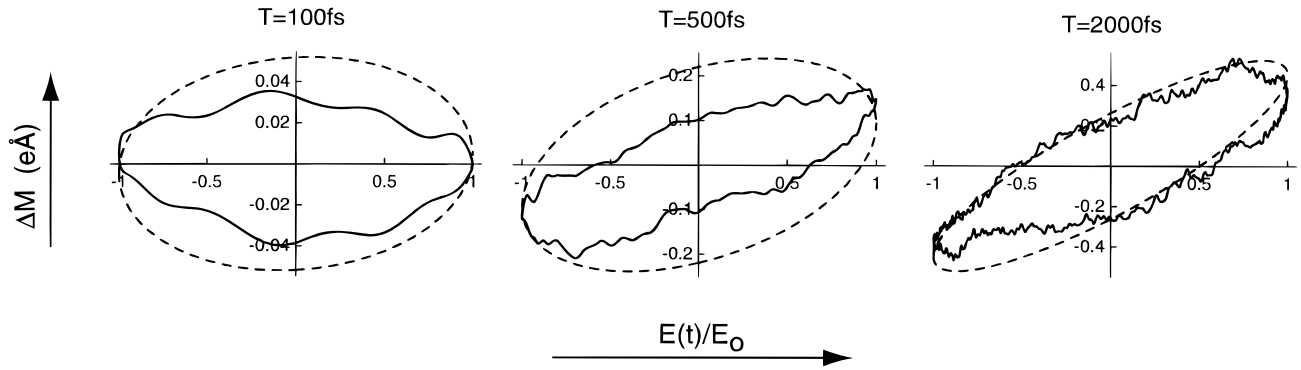

Figure 8. $E(t)/E_0$, $\langle \Delta M \rangle(t)$, diagram of the protein BPTI demonstrating hysteretic behavior in a periodic (spatially homogenous) external field $E(t) = E_0 \sin(2\pi t/t_p)$, for $t_p = 100$, 500, and 2000 fs. $E(t)$ is the external electric field applied to the protein at time t, and $\langle \Delta M \rangle(t)$ is the corresponding change of dipole moment per cycle averaged over all cycles in a 200 ps simulation. The solid lines correspond to $\langle \Delta M \rangle(t)$ evaluated such and the broken lines to $\langle \Delta M \rangle(t)$ evaluated according to (65).

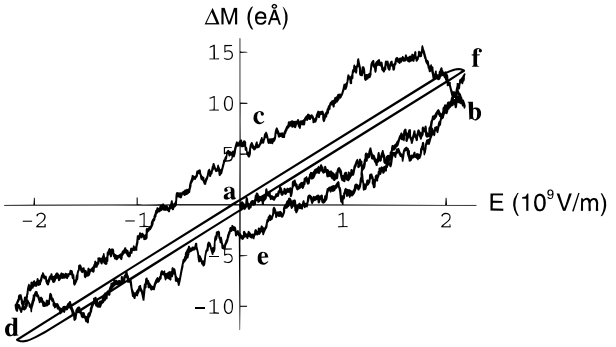

Figure 9. $E(t)$, $\Delta M(t)$ diagram of the protein BPTI demonstrating hysteretic behavior in a cyclic electric field. $E(t)$ is the external electric field applied to the protein at time t, and $\Delta M(t)$ is the corresponding change of dipole moment. The applied cyclic electric field is $E(t) = E_0 t/t_0$ for $0 \le t < t_0$ (a → b); $E(t) = E_0(2t_0 - t)/t_0$ for $t_0 \le t < 3t_0$ (b → c → d); $E(t) = E_0(t - 4t_0)/t_0$ for $3t_0 \le t \le 5t_0$ (d → e → f), for $E_0 = 2.17 \times 10^9$ V/m and $t_0 = 5$ ps; $T_0 = 100$ K. Jagged line: simulation data; smooth line: description by means of (64).

the 25 ps duration of the hysteresis loop in Figure 9; otherwise the loop would have narrowed. A model, derived further below, based solely on the dipolar relaxation time $\tau_0 = 0.185$ ps in (8) and the properties σ_M, χ_e in (7), (11), and (14) yields, in fact, a narrow hysteresis loop as shown in Figure 9. This implies that the protein exhibits at least two dipolar relaxation times: a short time $\tau_0 = 0.185$ ps reflected in dipolar fluctuations as analyzed through the dipole autocorrelation function shown in Figure 2, and a time of 100 ps or longer, documented in Figure 4. The latter time governs structural transitions among multiple metastable states of the protein induced by the external field.

F. Dipolar Response to a Brief Field Pulse. In Figure 4 we have presented, in terms of RMSD values, the structural changes which BPTI experiences after electric field pulses of the form

$$\vec{E}(t) = \begin{cases} 0 & t < 0 \text{ or } t > \tau \\ E_0 \hat{x} & 0 \le t \le \tau \end{cases} \qquad (18)$$

for $\tau = 1$, 2, and 3 ps and $E_0 \le 2.17 \times 10^9$ V/m. The shortest (1 ps) pulse was found not to induce permanent structural changes as judged by a comparison of RMSD values of BPTI for a field free simulation. In the following we consider the application of field pulses of short duration, $\tau \le 2$ ps. One expects in this case that the structure of BPTI remains unaltered for the shorter pulses or for sufficiently weak fields. We will monitor the behavior of the protein through its dipolar response, i.e., through the change in dipole moment $\Delta M(t)$ (in the direction of the applied field) during and after the pulse. One expects that $\Delta M(t)$ briefly rises from an initial zero value and then decays back to zero again, except in the case of longer and stronger pulses. Typically, the fluctuations of the dipole moment stemming from a single MD trajectory are large. In order to reveal $\Delta M(t)$ beneath the thermal fluctuations, we carried out simulations for different initial conditions and determined $\Delta M(t)$ averaged over several such trajectories.

Figure 10 shows the dipole moment response to a brief (0.6 ps) field pulse as described by (18). The temperature of the system is not raised significantly through the pulse. The dipole moment relaxation can be described well by

$$M(t) - \langle M \rangle = [M(\tau) - \langle M \rangle] C_{M,M}(t - \tau) \qquad (19)$$

for 0.6 ps $< t <$ 2.5 ps but starts to deviate thereafter. $\langle M \rangle$ in (19) is the averaged dipole moment before the field pulse. The rationale of (19) will be discussed further below. The maximum error of the dipole moment for 2.5 ps $< t <$ 5.0 ps is ± 0.30 e Å; hence, the deviation between the relaxation and (19) is statistically significant.

Figure 11 demonstrates the dipole moment relaxation for a long (2 ps) field pulse. The results show a strong deviation from (19). The deviation is largest during the interval 3 ps $< t <$ 4 ps. Since the deviation is localized in time, we refer to this deviation as a *dipole echo*. The maximum error of the dipole moment for 2.5 ps $< t <$ 4.5 ps is ± 0.47 e Å, which indicates that the dipole echo is statistically significant.

Figure 12 shows the dipole moment response for a strong field and a brief (0.25 ps) pulse. The strong field induces a large temperature change. The relaxation of the dipole moment cannot be described well by (19). A dipole echo is observed at $t \approx 0.65$ ps. The echo at $t \approx 0.65$ ps is also observed under a much weaker field of 10^8 V/m lasting for 0.25 ps, as shown in Figure 13. To obtain significant $\Delta M(t)$ values hidden beneath thermal fluctuations, we carried out again a pair of simulations starting from identical initial positions and velocities, the latter generated for $T_0 = 100$ K. After 1 ps dynamics one simulation continued without a field while an external field of 1.00×10^8 V/m was applied in the other simulation. $\Delta M(t)$ was evaluated from the difference of the total dipole moments of BPTI as described by the two simulations. Fourteen pairs of such simulations were carried out, and averages as well as error bars were determined. Although the resulting relative errors are large, it is evident that the dipole relaxation indeed exhibits significant deviations from (19).

IV. Theory

In this section we provide an analytical description of the dipole echo and hysteresis effect, illustrate the theory through

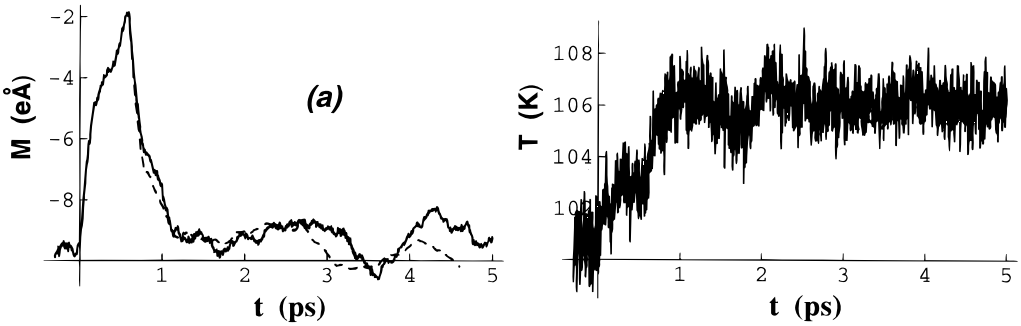

Figure 10. (a) Response of the dipole moment of BPTI along the direction of an applied electric field pulse described by (18), with $E_0 = 1.74 \times 10^9$ V/m and $\tau = 0.6$ ps. The broken line represents the prediction due to (19), employing the dipole autocorrelation function shown in Figure 2. (b) Temperature changes accompanying (a). The dipole moment and temperature were averaged over ten molecular dynamics trajectories with different initial conditions.

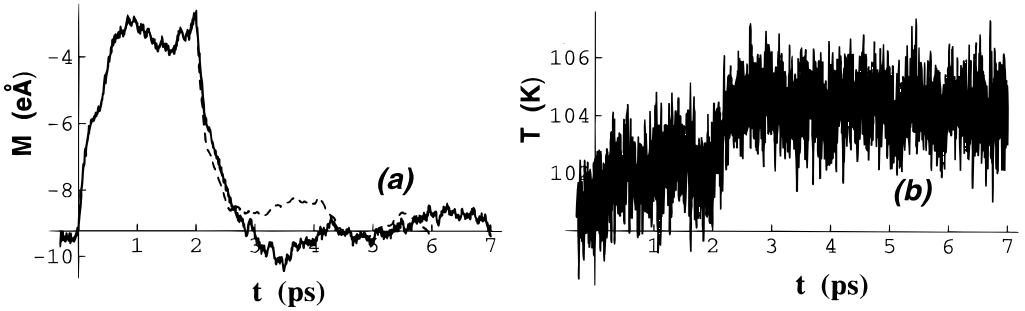

Figure 11. (a) Response of the dipole moment of BPTI along the direction of an applied electric field described by (18), with $E_0 = 1.31 \times 10^9$ V/m and $\tau = 2$ ps. The broken line represents the prediction due to (19), employing the dipole autocorrelation function shown in Figure 2. At $t \approx 3.5$ ps, a significant deviation (echo) between the actual response and the description of (19) is observed. (b) Temperature changes accompanying (a). The response shown was averaged over seven molecular dynamics trajectories.

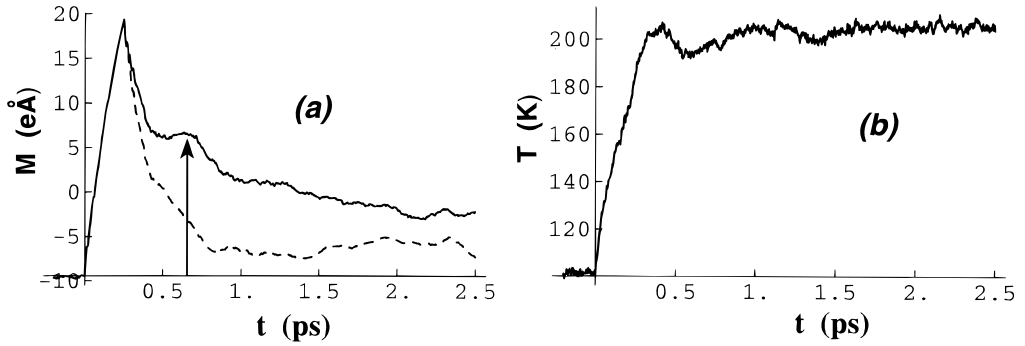

Figure 12. (a) Response of the dipole moment of BPTI along the direction of an applied electric field described by (18), with $E_0 = 8.69 \times 10^9$ V/m and $\tau = 0.25$ ps. The broken line represents the prediction due to (19), employing the dipole autocorrelation function shown in Figure 2. (b) Temperature changes accompanying (a). The dipole moment and temperature shown are averaged over seven initial conditions. The maximum error of the dipole moment for $t > 0.25$ ps is ± 1.77 e Å.

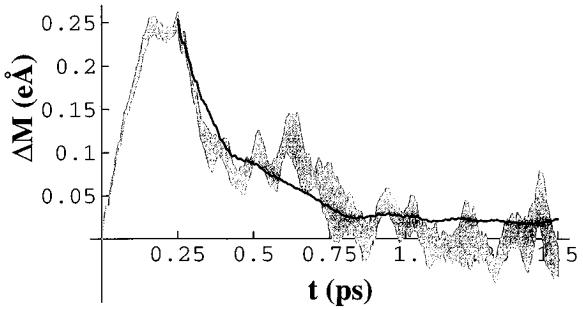

Figure 13. Dipole moment of BPTI along the direction of an applied field described by (18), with $E_0 = 1 \times 10^8$ V/m and $\tau = 0.25$ ps, relative to the dipole moment of BPTI not experiencing an external field. The simulations of the two cases started with identical initial positions and velocities, the latter generated for $T_0 = 100$ K. The dipolar response has been averaged over 14 molecular dynamics trajectories with different initial conditions. The gray region indicates the range of $\Delta M(t)$ values based on the determined average and standard deviation. The dark line represents the prediction due to (19), employing the dipole autocorrelation function shown in Figure 2.

sample cases, and compare the theory's predictions with simulation results. In the following derivation we determine first how the average *x*-coordinate of each atom, i.e., the atom's coordinate in the direction of the applied field, evolves under perturbations described by eq 18. In refs 29, 30, and 40 it had been demonstrated that an ensemble of Langevin oscillators provides a satisfactory description of motions in BPTI over time scales of a few picoseconds and averaged over many degrees of freedom. Following refs 29, 30, and 40, we apply the Langevin oscillator model here to account for the dipolar relaxation in BPTI. We then describe dipolar hysteresis, assuming models which describe the dipolar dynamics of a protein through a one-dimensional Fokker−Planck equation.

A. Three Stages of Normal Mode Dynamics. In order to obtain expressions for the dipole moment of an ensemble of Langevin oscillators in the presence of the electric field (18), we divide the dynamics into three stages, i.e., stage "0" before the electric field pulse, stage "1" during the field pulse, and stage "2" after the field pulse.

(0) Before the Field Pulse. $X_\alpha(t)$ denotes the coordinate of the αth atom or mode of the ensemble, and $\langle X_\alpha(t)\rangle$ denotes its time average. We define $x_{\alpha,0} = \langle X_\alpha(t)\rangle$ and focus on the deviation from the average defined through

$$x_\alpha(t) = X_\alpha(t) - x_{\alpha,0} \tag{20}$$

The motion of the αth atom or mode is governed by the Langevin equation

$$\frac{d^2x_\alpha^{(0)}}{dt^2} + b_\alpha \frac{dx_\alpha^{(0)}}{dt} + \omega_\alpha{}^2 x_\alpha^{(0)} = A_\alpha(t) \tag{21}$$

which describes a harmonic motion in the presence of frictional and fluctuating forces. ω_α is the frequency of the oscillator, b_α is the friction constant, and $A_\alpha(t)$ is the fluctuating force which is assumed to be δ-correlated. The amplitude of the fluctuating force, according to the fluctuation−dissipation theorem, is related to the friction coefficient through

$$\langle A_\alpha(0)\, A_\alpha(t)\rangle = 2k_B T_0 b_\alpha \delta(t)/m_\alpha \tag{22}$$

According to our model the average of the initial coordinates is

$$\langle x_\alpha^{(0)}(0)\rangle_{(0)} = 0 \tag{23}$$

The average of the initial velocities, which are Maxwell-

distributed, obeys

$$\langle v_\alpha^{(0)}(0)\rangle_{(0)} = 0 \tag{24}$$

Here $\langle ...\rangle_{(0)}$ denotes the average during the stage before the field pulse.

The equilibrium correlation function of the individual modes, in the case of underdamped motion, i.e., for $\omega_\alpha > {}^1/_2 b_\alpha$, is given by the expression[41]

$$\langle x_\alpha^{(0)}(t)\, x_\lambda^{(0)}(0)\rangle_{(0)} = \frac{k_B T_0 e^{-b_\alpha t/2}}{m_\alpha \omega_\alpha{}^2}\left(\cos(\Omega_\alpha t) + \frac{b_\alpha}{2\Omega_\alpha}\sin(\Omega_\alpha t)\right)\delta_{\alpha,\lambda} \tag{25}$$

where

$$\Omega_\alpha = \left[\omega_\alpha{}^2 - \frac{1}{4} b_\alpha{}^2\right]^{1/2} \tag{26}$$

Accordingly, the RMSD of the mode is initially

$$\langle [x_\alpha^{(0)}(0)]^2\rangle_{(0)} = k_B T_0 / m_\alpha \omega_\alpha{}^2 \tag{27}$$

and the normalized equilibrium correlation function is

$$C_{x,x}(t) = e^{-b_\alpha t/2}\left(\cos(\Omega_\alpha t) + \frac{b_\alpha}{2\Omega_\alpha}\sin(\Omega_\alpha t)\right) \tag{28}$$

Comparison with the correlation functions in Figure 6 for three representative atoms of BPTI, evaluated by means of molecular dynamics simulations, shows that the motions are indeed underdamped since they exhibit a few oscillations.

For the sake of simplicity we assume $q_0 = 0$ in (3); i.e., we assume that the total charge of the ensemble vanishes. The total dipole moment is then

$$M^{(0)}(t) = \sum_\alpha [q_\alpha x_\alpha^{(0)}(t) + q_\alpha x_{\alpha,0}^{(0)}] \tag{29}$$

For the time average of this expression it holds, due to $\langle x_\alpha^{(0)}(t)\rangle_t = 0$, that

$$\langle M^{(0)}\rangle_t = \sum_\alpha q_\alpha x_{\alpha,0}^{(0)} \tag{30}$$

From this follows

$$\langle (M^{(0)}(t) - \langle M^{(0)}\rangle_t)(M^{(0)}(0) - \langle M^{(0)}\rangle_t)\rangle_{(0)} = \langle (\sum_\alpha q_\alpha x_\alpha^{(0)}(t))(\sum_\lambda q_\lambda x_\lambda^{(0)}(0))\rangle_{(0)}$$

$$= \sum_\alpha \frac{k_B T_0 q_\alpha{}^2 e^{-b_\alpha t/2}}{m_\alpha \omega_\alpha{}^2}\left(\cos(\Omega_\alpha t) + \frac{b_\alpha}{2\Omega_\alpha}\sin(\Omega_\alpha t)\right) \tag{31}$$

We conclude that the dipole moment autocorrelation function $C_{M,M}(t)$, in the absence of the electric field, according to (4), is

$$C_{M,M}(t) = \frac{1}{\sum_\alpha q_\alpha{}^2/m_\alpha \omega_\alpha{}^2}\sum_\alpha \frac{q_\alpha{}^2 e^{-b_\alpha t/2}}{m_\alpha \omega_\alpha{}^2}\left(\cos(\Omega_\alpha t) + \frac{b_\alpha}{2\Omega_\alpha}\sin(\Omega_\alpha t)\right) \tag{32}$$

(1) During the Field Pulse. With the electric field applied, the coordinate of the αth atom or mode is governed by the Langevin equation with added homogeneous force, with a modified frequency $\tilde{\omega}_\alpha$ and with a modified friction constant $\tilde{b}_\alpha$

$$\frac{d^2 x_\alpha^{(1)}}{dt^2} + \tilde{b}_\alpha \frac{dx_\alpha^{(1)}}{dt} + \tilde{\omega}_\alpha{}^2 x_\alpha^{(1)} = A_\alpha(t) + \frac{q_\alpha E_0}{m_\alpha} \tag{33}$$

The assumption of modified frequency and friction is motivated by the results shown in Figure 6. This figure demonstrates that the position autocorrelation functions and, hence, atomic vibrations with and without the external electric field are significantly different. For this reason modified friction constants and frequencies are employed for the period during which the field pulse is applied.

The added force corresponds to a new potential

$$V_\alpha(x_\alpha) = \frac{1}{2} m_\alpha \tilde{\omega}_\alpha{}^2 [x_\alpha^{(1)}]^2 - q_\alpha E_0 x_\alpha^{(1)} \tag{34}$$

which can be written as a shifted harmonic oscillator potential

$$V_\alpha(x_\alpha) = \frac{1}{2} m_\alpha \tilde{\omega}_\alpha{}^2 \left[x_\alpha^{(1)} - \frac{q_\alpha E_0}{m_\alpha \tilde{\omega}_\alpha{}^2}\right]^2 - \frac{q_\alpha{}^2 E_0{}^2}{2 m_\alpha \tilde{\omega}_\alpha{}^2} \tag{35}$$

Accordingly, one can simplify the Langevin equation (33) by introducing the new coordinate

$$y_\alpha^{(1)} = x_\alpha^{(1)} - \frac{q_\alpha E_0}{m_\alpha \tilde{\omega}_\alpha{}^2} \tag{36}$$

to obtain, instead of eq 33,

$$\frac{d^2 y_\alpha^{(1)}}{dt^2} + \tilde{b}_\alpha \frac{dy_\alpha^{(1)}}{dt} + \tilde{\omega}_\alpha{}^2 y_\alpha^{(1)} = A_\alpha(t) \tag{37}$$

Assuming that all modes remain underdamped, one defines the real quantity

$$\tilde{\Omega}_\alpha = \left[\tilde{\omega}_\alpha{}^2 - \frac{1}{4}\tilde{b}_\alpha{}^2\right]^{1/2} \tag{38}$$

The autocorrelation function corresponding to the Langevin equation (37) is again given by (28), albeit with modified constants $\tilde{\Omega}_\alpha$ and $\tilde{b}_\alpha$.

The averaged coordinate $y_\alpha^{(1)}(t)$ and velocity $v_\alpha^{(1)}(t)$, during the field pulse, can be expressed according to (214) in ref 42

$$\langle y_\alpha^{(1)}(t)\rangle_{(1)} = y_\alpha^{(0)}(0) e^{-\tilde{b}_\alpha t/2}\left(\cos(\tilde{\Omega}_\alpha t) + \frac{\tilde{b}_\alpha}{2\tilde{\Omega}_\alpha}\sin(\tilde{\Omega}_\alpha t)\right) + \frac{v_\alpha^{(0)}(0)}{\tilde{\Omega}_\alpha} e^{-\tilde{b}_\alpha t/2}\sin(\tilde{\Omega}_\alpha t) \tag{39}$$

$$\langle v_\alpha^{(1)}(t)\rangle_{(1)} = -\frac{y_\alpha^{(0)}(0)\tilde{\omega}_\alpha{}^2}{\tilde{\Omega}_\alpha} e^{-\tilde{b}_\alpha t/2}\sin(\tilde{\Omega}_\alpha t) + v_\alpha^{(0)}(0) e^{-\tilde{b}_\alpha t/2}\left[\cos(\tilde{\Omega}_\alpha t) - \frac{\tilde{b}_\alpha}{2\tilde{\Omega}_\alpha}\sin(\tilde{\Omega}_\alpha t)\right] \tag{40}$$

where $y_\alpha^{(0)}(0)$ and $v_\alpha^{(0)}(0)$ are the initial coordinates and velocities. Here $\langle ...\rangle_{(1)}$ denotes the average during the electric pulse.

Averaging over the initial coordinate, i.e., employing

$$\langle y_\alpha^{(0)}(0)\rangle_{(0)} = \langle x_\alpha^{(0)}(0)\rangle_{(0)} - \frac{q_\alpha E_0}{m_\alpha \tilde{\omega}_\alpha{}^2} = -\frac{q_\alpha E_0}{m_\alpha \tilde{\omega}_\alpha{}^2} \quad (41)$$

yields

$$\langle\langle y_\alpha^{(1)}(\tau)\rangle_{(1)}\rangle_{(0)} = -\frac{q_\alpha E_0}{m_\alpha \tilde{\omega}_\alpha{}^2}\, \mathrm{e}^{-\tilde{b}_\alpha \tau/2}\left(\cos(\tilde{\Omega}_\alpha \tau) + \frac{\tilde{b}_\alpha}{2\tilde{\Omega}_\alpha}\sin(\tilde{\Omega}_\alpha \tau)\right) \quad (42)$$

$$\langle\langle v_\alpha^{(1)}(\tau)\rangle_{(1)}\rangle_{(0)} = \frac{q_\alpha E_0}{m_\alpha \tilde{\Omega}_\alpha}\, \mathrm{e}^{-\tilde{b}_\alpha \tau/2}\sin(\tilde{\Omega}_\alpha \tau) \quad (43)$$

Equation (42) can be expressed in terms of the coordinates $x_\alpha^{(1)}$

$$\langle\langle x_\alpha^{(1)}(\tau)\rangle_{(1)}\rangle_{(0)} = \frac{q_\alpha E_0}{m_\alpha \tilde{\omega}_\alpha{}^2} - \frac{q_\alpha E_0}{m_\alpha \tilde{\omega}_\alpha{}^2}\mathrm{e}^{-\tilde{b}_\alpha \tau/2}\left(\cos(\tilde{\Omega}_\alpha \tau) + \frac{\tilde{b}_\alpha}{2\tilde{\Omega}_\alpha}\sin(\tilde{\Omega}_\alpha \tau)\right) \quad (44)$$

In this expression the first term on the right hand side describes the adiabatic value of the coordinate, which arises for slowly varying potentials or after the system has been equilibrated in the presence of the applied field; the second term describes the relaxation of the coordinate and contains the memory of the system about its state before the potential was applied.

(2) After the Field Pulse. After the electric field is turned off at time $t = \tau$, the protein relaxes to the state before the electric pulse, except that the temperature of the protein is raised through the pulse. In case the temperature increase is small, one can assume that the system is governed by the same Langevin equation as before the application of the pulse, namely, by

$$\frac{\mathrm{d}^2 x_\alpha^{(2)}}{\mathrm{d}t^2} + b_\alpha \frac{\mathrm{d}x_\alpha^{(2)}}{\mathrm{d}t} + \omega_\alpha{}^2 x_\alpha^{(2)} = A_\alpha(t) \quad (45)$$

The average of $x_\alpha^{(2)}(t)$, for initial positions and velocities given by $x_\alpha^{(1)}(\tau)$ and $v_\alpha^{(1)}(\tau)$, is [cf. (39)]

$$\langle x_\alpha^{(2)}(t)\rangle_{(2)} = x_\alpha^{(1)}(\tau)\mathrm{e}^{-b_\alpha(t-\tau)/2}\left[\cos(\Omega_\alpha(t-\tau)) + \frac{b_\alpha}{2\Omega_\alpha}\sin(\Omega_\alpha(t-\tau))\right] + \frac{v_\alpha^{(1)}(\tau)}{\Omega_\alpha}\mathrm{e}^{-b_\alpha(t-\tau)/2}\sin(\Omega_\alpha(t-\tau)) \quad (46)$$

This expression needs to be averaged over the initial coordinates and velocities $x_\alpha^{(1)}(\tau)$ and $v_\alpha^{(1)}(\tau)$, for which purpose one can employ (43) and (44). Defining $t' = t - \tau$, one obtains for the average position after application of the field pulse

$$\langle\langle\langle x_\alpha^{(2)}(t')\rangle_{(2)}\rangle_{(1)}\rangle_{(0)} = \frac{q_\alpha E_0}{m_\alpha \tilde{\omega}_\alpha{}^2}\mathrm{e}^{-b_\alpha t'/2}\left(\cos(\Omega_\alpha t') + \frac{b_\alpha}{2\Omega_\alpha}\sin(\Omega_\alpha t')\right)\left[1 - \mathrm{e}^{-\tilde{b}_\alpha \tau/2}\left(\cos(\tilde{\Omega}_\alpha \tau) + \frac{\tilde{b}_\alpha}{2\tilde{\Omega}_\alpha}\sin(\tilde{\Omega}_\alpha \tau)\right)\right] + \frac{q_\alpha E_0}{m_\alpha \Omega_\alpha \tilde{\Omega}_\alpha}\mathrm{e}^{-\tilde{b}_\alpha \tau/2}\sin(\tilde{\Omega}_\alpha \tau)\mathrm{e}^{-b_\alpha t'/2}\sin(\Omega_\alpha t') \quad (47)$$

This expression can be separated into a contribution $\tilde{x}_\alpha^{(2)}(t')$ which is the limit for $\tau \to \infty$ and a remaining contribution $\Delta x_\alpha^{(2)}(t)$, i.e.,

$$\langle\langle\langle x_\alpha^{(2)}(t')\rangle_{(2)}\rangle_{(1)}\rangle_{(0)} = \langle\langle\langle \tilde{x}_\alpha^{(2)}(t')\rangle_{(2)}\rangle_{(1)}\rangle_{(0)} + \langle\langle\langle \Delta x_\alpha^{(2)}(t')\rangle_{(2)}\rangle_{(1)}\rangle_{(0)} \quad (48)$$

where

$$\langle\langle\langle \tilde{x}_\alpha^{(2)}(t')\rangle_{(2)}\rangle_{(1)}\rangle_{(0)} = \frac{q_\alpha E_0}{m_\alpha \tilde{\omega}_\alpha{}^2}\exp\left(\frac{-b_\alpha t'}{2}\right)\left(\cos(\Omega_\alpha t') + \frac{b_\alpha}{2\Omega_\alpha}\sin(\Omega_\alpha t')\right) \quad (49)$$

$$\langle\langle\langle \Delta x_\alpha^{(2)}(t')\rangle_{(2)}\rangle_{(1)}\rangle_{(0)} = \frac{q_\alpha E_0}{m_\alpha \tilde{\omega}_\alpha{}^2}\exp\left(-\frac{b_\alpha t' + \tilde{b}_\alpha \tau}{2}\right)\left[\frac{b_\alpha}{2\Omega_\alpha} \times \sin(\Omega_\alpha t' + \tilde{\Omega}_\alpha \tau) + \cos(\tilde{\Omega}_\alpha \tau)\cos(\Omega_\alpha t') - \frac{4\tilde{\omega}_\alpha{}^2 - b_\alpha \tilde{b}_\alpha}{4\Omega_\alpha \tilde{\Omega}_\alpha} \times \sin(\tilde{\Omega}_\alpha \tau)\sin(\Omega_\alpha t')\right] \quad (50)$$

The latter expression can be written

$$\langle\langle\langle \Delta x_\alpha^{(2)}(t')\rangle_{(2)}\rangle_{(1)}\rangle_{(0)} = -\frac{q_\alpha E_0}{m_\alpha \tilde{\omega}_\alpha{}^2}\exp\left(-\frac{b_\alpha t' + \tilde{b}_\alpha \tau}{2}\right)\left[\frac{b_\alpha}{2\Omega_\alpha} \times \sin(\Omega_\alpha t' + \tilde{\Omega}_\alpha \tau) + \frac{4\Omega_\alpha \tilde{\Omega}_a - 4\tilde{\omega}_\alpha{}^2 + b_\alpha \tilde{b}_\alpha}{8\Omega_\alpha \tilde{\Omega}_\alpha}\cos(\Omega_\alpha t' - \tilde{\Omega}_\alpha \tau) + \frac{4\Omega_\alpha \tilde{\Omega}_\alpha + 4\tilde{\omega}_\alpha{}^2 - b_\alpha \tilde{b}_\alpha}{8\Omega_\alpha \tilde{\Omega}_\alpha}\cos(\Omega_\alpha t' + \tilde{\Omega}_\alpha \tau)\right] \quad (51)$$

B. Dipole Echo. $\tilde{M}_\alpha^{(2)}(t')$ denotes the dipole moment corresponding to $x_\alpha^{(0)}$ and $\tilde{x}_\alpha^{(2)}(t')$, and $\Delta M_\alpha^{(2)}(t)$ is the dipole moment corresponding to $\Delta x_\alpha^{(2)}(t)$. One obtains for the first contribution in (48) the dipole moment

$$\tilde{M}^{(2)}(t') - \langle M^{(0)}\rangle = \sum_{\alpha=1}^{N}\langle\langle\langle q_\alpha \tilde{x}_\alpha^{(2)}(t)\rangle_{(2)}\rangle_{(1)}\rangle_{(0)}$$

$$= \sum_{\alpha=1}^{N}\frac{q_\alpha{}^2 E_0}{m_\alpha \tilde{\omega}_\alpha{}^2}\exp\left(\frac{-b_\alpha t'}{2}\right)\left(\cos(\Omega_\alpha t') + \frac{b_\alpha}{2\Omega_\alpha}\sin(\Omega_\alpha t')\right) \quad (52)$$

In the case $\tilde{\omega}_\alpha = \omega_\alpha$ and $\tilde{b}_\alpha = b_\alpha$ this yields [cf. (32)]

$$\tilde{M}^{(2)}(t') - \langle M^{(0)}\rangle = \sum_{\alpha=1}^{N}\frac{q_\alpha{}^2 E_0}{m_\alpha \omega_\alpha{}^2}\exp\left(\frac{-b_\alpha t'}{2}\right)\left(\cos(\Omega_\alpha t') + \frac{b_\alpha}{2\Omega_\alpha}\sin(\Omega_\alpha t')\right)$$

$$\propto C_{M,M}(t') \quad (53)$$

This result matches (19).

We consider now the contribution to the total dipole moment due to $\Delta x_\alpha^{(2)}(t)$. One obtains from (51)

$$\Delta M^{(2)}(t') = \sum_{\alpha=1}^{N}\left\{-\frac{{q_\alpha}^2 E_0}{m_\alpha {\tilde\omega_\alpha}^2}\exp\left(-\frac{b_\alpha t' + \tilde b_\alpha \tau}{2}\right)\left[\frac{b_\alpha}{2\Omega_\alpha}\sin(\Omega_\alpha t' + \tilde\Omega_\alpha \tau) + \frac{4\Omega_\alpha\tilde\Omega_\alpha + 4{\tilde\omega_\alpha}^2 - b_\alpha\tilde b_\alpha}{8\Omega_\alpha\tilde\Omega_\alpha}\cos(\Omega_\alpha t' + \tilde\Omega_\alpha\tau)\right]\right\} \quad (54)$$

Given $\tilde\omega_\alpha \approx \omega_\alpha$ and $\tilde b_\alpha \approx b_\alpha$, this is approximately

$$\sum_{\alpha=1}^{N}\left\{-\frac{{q_\alpha}^2 E_0}{m_\alpha {\omega_\alpha}^2}\exp\left[-\frac{b_\alpha(t'+\tau)}{2}\right]\left[\cos(\Omega_\alpha(t'+\tau)) + \frac{b_\alpha}{2\Omega_\alpha}\sin(\Omega_\alpha(t'+\tau))\right]\right\} \propto C_{M,M}(t'+\tau) \quad (55)$$

This expression represents the dipole autocorrelation function which decays with a relaxation time τ_0, except for a small number of residual oscillations. Hence, the expression above vanishes for $\tau \gg \tau_0$.

Actually, the contribution (55) to the dipole moment is expected to be vanishingly small if the external field is not too strong, even if $\tilde\omega_\alpha$ and $\tilde b_\alpha$ differ from ω_α and b_α, respectively. One may, hence, subtract this expression from the right hand side of (54). This results in

$$\Delta M^{(2)}(t') = \sum_{\alpha=1}^{N}\langle\langle\langle q_\alpha \Delta x_\alpha^{(2)}(t)\rangle_{(2)}\rangle_{(1)}\rangle_{(0)}$$

$$\approx \sum_{\alpha=1}^{N}\frac{{q_\alpha}^2 E_0}{m_\alpha{\tilde\omega_\alpha}^2}\frac{4{\tilde\omega_\alpha}^2 - b_\alpha\tilde b_\alpha - 4\Omega_\alpha\tilde\Omega_\alpha}{8\Omega_\alpha\tilde\Omega_\alpha}\exp\left(-\frac{b_\alpha t' + \tilde b_\alpha\tau}{2}\right)\times \cos(\Omega_\alpha t' - \tilde\Omega_\alpha\tau) \quad (56)$$

Note that this expression vanishes identically for $\tilde\omega_\alpha = \omega_\alpha$ and $\tilde b_\alpha = b_\alpha$. In this case the dipolar response of the ensemble is solely due to (53); i.e., the dipole moment relaxation after a field pulse can be represented by (19) for $\tilde\omega_\alpha = \omega_\alpha$ and $\tilde b_\alpha = b_\alpha$. Equation (56) describes a transient dipole moment, termed the dipole echo, arising beyond the contribution given by (53) or, equivalently, (19). The dipole echo term (56) vanishes for weak fields, i.e., for $\tilde\omega_\alpha \approx \omega_\alpha$ and $\tilde b_\alpha \approx b_\alpha$, and we have hence proven the relationship (19) in the weak field limit. Conversely, if the difference between $\tilde\omega_\alpha$ and ω_α is significantly large, (53) and (19) are no longer valid.

C. Comparison with Simulations. We have demonstrated that a dipolar response of an ensemble of Langevin oscillators is captured well by (19), i.e., by $C_{M,M}(t)$, as long as the applied field does not affect frequencies and friction constants. If these attributes are affected, one expects a contribution from those atoms or modes for which $4{\tilde\omega_\alpha}^2 - b_\alpha\tilde b_\alpha - 4\Omega_\alpha\tilde\Omega_a$ deviates significantly from zero. Such contributions show a maximum deviation from (19) for $\cos(\Omega_\alpha t' - \tilde\Omega_\alpha\tau) = 1$. If there are many modes which have a similar ratio of $\tilde\Omega_\alpha/\Omega_\alpha$, an echo will occur in the dipolar response at a time determined through $t' = \tilde\Omega_\alpha\tau/\Omega_\alpha$. That such behavior can indeed arise is demonstrated in the results shown in Figures 11 and 12. In the case in which the ratios $\tilde\Omega_\alpha/\Omega_\alpha$ are very heterogeneous for different α's, the deviation from (19) can exhibit an oscillatory behavior, as demonstrated in Figure 10.

The dipole moment response after a strong field pulse can result in a significant deviation from (19) even without considering the dipole echo. It seems that the continuous shift between the dipole relaxation and (19) shown in Figure 12 is due to such an effect when a strong external field makes $\tilde\omega_\alpha$ and ω_α strongly different.

In the case $\tilde b_\alpha = b_\alpha$ holds $4{\tilde\omega_\alpha}^2 - b_\alpha\tilde b_\alpha - 4\Omega_\alpha\tilde\Omega_\alpha = 4\tilde\Omega_\alpha(\tilde\Omega_\alpha - \Omega_\alpha)$. For $\tilde\Omega_\alpha < \Omega_\alpha$, the echo contribution of the αth mode in (56) is opposite to the external field and occurs at time $t' = \tilde\Omega_\alpha\tau/\Omega_\alpha < \tau$ and *vice versa*. This interesting feature is revealed in our simulations. It is shown in Figure 12 that a positive echo (in the direction of the external field) arises at $t' > \tau$, while a negative echo occurs at $t' < \tau$, as shown in Figure 11.

D. Numerical Experiments in Terms of Normal Mode Dynamics. In order to confirm whether the key features observed in the simulations of dipole echoes can be reproduced by (52) and (56), we consider an ensemble of Langevin oscillators exposed to a field pulse. For this purpose we assume an ensemble of 100 Langevin oscillators with Ω_α, $\alpha = 1, 2, ..., 100$, and block-shaped density; i.e., the Ω_α are uniformly distributed in the range $0.4\ t_o^{-1} < \Omega < 4.0\ t_o^{-1}$, where t_o is the time unit. We selected, accordingly, a set of 100 random Ω_α obeying the stated density. The reason why we chose the sampling of Ω_α rather than ω_α is that we would like to test directly the mechanism of dipole echoes as pointed out earlier; i.e., we consider a situation in which many modes which have a similar ratio $\tilde\Omega_\alpha/\Omega_\alpha$ contribute an echo at the time $t' = \tilde\Omega_\alpha\tau/\Omega_\alpha$.

The prefactor ${q_\alpha}^2E_0/m_\alpha$ in (52) and (56) is independent of the remaining constants in these equations. For the sake of simplicity, we choose ${q_\alpha}^2E_0/m_\alpha = s_o t_o^{-2}$ for all the modes, where s_o is the unit of dipole moment. Furthermore, we assume $\tilde b_\alpha = b_\alpha = b = 0.01 t_o^{-1}$ and choose the parameter $c = \tilde\Omega_\alpha/\Omega_\alpha$ to be independent of α. Then $\tilde\Omega_\alpha$ is known from c, and Ω_a, and $\tilde\omega_\alpha$ can be determined from (38). Hence (52) and (56) can be rewritten

$$\tilde M^{(2)}(t') - \langle M^{(0)}\rangle = \frac{s_o}{{t_o}^2}\sum_{\alpha=1}^{100}\frac{1}{{\tilde\omega_\alpha}^2}\exp\left(\frac{-bt'}{2}\right)\left(\cos(\Omega_\alpha t') + \frac{b}{2\Omega_\alpha}\sin(\Omega_\alpha t')\right) \quad (57)$$

$$\Delta M^{(2)}(t') = \frac{(c-1)s_o}{2{t_o}^2}\sum_{\alpha=1}^{100}\frac{1}{{\tilde\omega_\alpha}^2}\exp\left[-\frac{b(t'+\tau)}{2}\right]\cos(\Omega_\alpha t' - \tilde\Omega_\alpha\tau) \quad (58)$$

and the total dipole moment $M^{(2)}(t')$ is

$$M^{(2)}(t') - \langle M^{(0)}\rangle = [\tilde M^{(2)}(t') - \langle M^{(0)}\rangle] + \Delta M^{(2)}(t') \quad (59)$$

We employed the program package Mathematica[43] to evaluate (57)−(59). Figure 14 presents the resulting dipole moments. The figure demonstrates that a dipole echo occurs at $t' = c\tau$. It also shows that for $c > 1$ the system generates a positive echo and for $c < 1$ it generates a negative echo. This behavior is consistent with the simulation results presented in Figures 11 and 12.

E. Hysteresis. We seek to relate now the hysteretic behavior of BPTI, as demonstrated in Figures 8 and 9, to basic properties of the protein. For this purpose we note that the response to

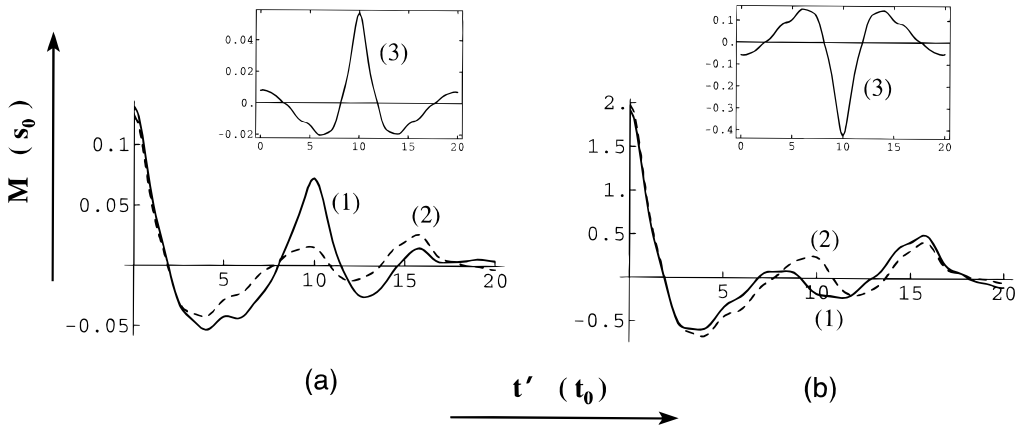

Figure 14. Response of the dipole moment of an ensemble of Langevin oscillators to an applied electric field pulse, calculated from (57)−(59). (1) represents the dipole moment $M^{(2)}(t') - \langle M^{(0)}\rangle$ in (59) (solid lines); (2) represents $\tilde{M}^{(2)}(t') - \langle M^{(0)}\rangle$ in (57) (broken lines); (3) represents $\Delta M^{(2)}(t')$ in (58) (inserts). The parameters are chosen for two cases: (a) $\tau = 5$ and $c = 2$; (b) $\tau = 20$ and $c = {}^1/_2$. t_o is the time unit, and s_o is the unit of dipole moment.

an external field, as derived above in the framework of the Langevin oscillator model, is actually given by the dipole moment autocorrelation function as long as field effects on frequencies and friction can be neglected. One can derive the identity of response and correlation function in linear response theory, i.e., for weak fields, also when the dipole fluctuations are governed by a Langevin equation or, equivalently, by a Fokker−Planck equation,[19] the approach we will take at present to describe dipolar hysteresis.

Figures 1 and 2 demonstrate that $M(t)$ can be approximated well by a stochastic process characterized through a Gaussian distribution

$$p_o(M) = \frac{1}{(2\pi)^{1/2}\sigma_M} \exp[-(M - M_o)^2/2{\sigma_M}^2] \qquad (60)$$

and a monoexponential correlation function (8). Such a process is known as an Ornstein−Uhlenbeck process.[44] We consider the dynamics of $\Delta M = M - M_0$. The probability $p(\Delta M,t)$ that for this quantity a value ΔM arises at time t is governed by the Fokker−Planck equation

$$\partial_t p(\Delta M,t) = \frac{1}{\tau_0}\,\partial_M[{\sigma_M}^2\,\partial_M + (\Delta M - \Delta M_0)]p(\Delta M,t) \qquad (61)$$

where, in the present case, $\Delta M_0 = 0$. It is worth noting that this corresponds to diffusion in the harmonic potential $U(\Delta M) = {}^1/_2(\Delta M - \Delta M_0)^2$ with the diffusion constant $D = {\sigma_M}^2/\tau_0$ and temperature ${\sigma_M}^2/k_B$.

Equation (61) also holds if ΔM_0 is modified by time-dependent external fields. From our knowledge of the adiabatic behavior of the system, we can write

$$\Delta M_0 = \alpha E; \quad \alpha = V\epsilon_0\chi_e \qquad (62)$$

where α is the so-called molecular polarizability of the system and E is the strength of an external homogenous field. We stress that this description of the protein's dielectric response is solely based on the properties σ_M, τ_0, and χ_e, given in (7), (8), (10), and (14) and determined through simulations of an equilibrated, field free protein.

A solution of (61) is given by

$$p(\Delta M,t) = \frac{1}{(2\pi)^{1/2}\sigma_M} \exp[-(\Delta M - \langle\Delta M\rangle(t))^2/2{\sigma_M}^2] \qquad (63)$$

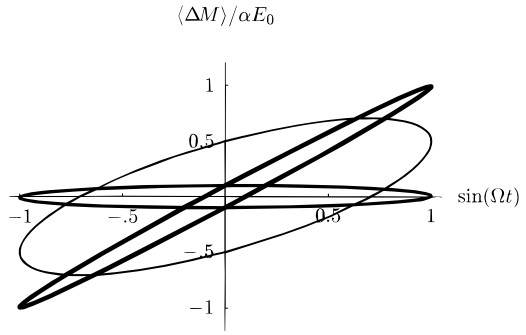

Figure 15. Hysteresis loop at high, moderate, and low driving frequencies as described by (65): medium line, high-frequency loop ($\omega = 10$); thin line, moderate-frequency loop ($\omega = 1$); thick line, low-frequency loop ($\omega = 0.1$). The hysteresis loops for the Ornstein−Uhlenbeck process are independent of σ.

where $\langle\Delta M\rangle(t)$ in turn is the solution of

$$\frac{d}{dt}\langle\Delta M\rangle = -\frac{1}{\tau_0}(\langle\Delta M\rangle - \alpha E(t)) \qquad (64)$$

In the case $\langle\Delta M\rangle(0) = 0$ the solution (63) coincides at $t = 0$ with (60), i.e., describes the response of a system initially in equilibrium. According to (63) the shape of the distribution does not change when a bias is applied to the system.

In the case of a periodic external field $E(t) = E_0 \sin(\Omega t)$ one can determine the asymptotic or "steady-state" behavior of the system from (63) by integrating (64) over many cycles of this field. One obtains (see ref 45 for further discussion of periodically driven Ornstein−Uhlenbeck processes)

$$\langle\Delta M\rangle(t) = \alpha E_0 \frac{\sin(\Omega t) - \omega\cos(\Omega t)}{1 + \omega^2}, \quad \omega = \tau_0\Omega \qquad (65)$$

Since $\langle\Delta M\rangle(t)$ represents the average value of $p(\Delta M,t)$ expression (65) provides directly the observed dipole moment of an ensemble of proteins. One may note that this solution does not depend on σ_M. The behavior of $\langle\Delta M\rangle(t)$ for various values of ω is illustrated in Figure 15. At both low and high driving frequencies there is little hysteresis, in the first case because the system has time to follow the applied field closely and in the second case because there is too little time to follow at all. Between these extremes is the region of high hysteresis in which the system is out of phase with the applied field.

The above prediction can be compared with simulations accounting for $\langle \Delta M \rangle(t)$ in the presence of a weak, sinusoidal field, as shown in Figure 8. The respective simulations were conducted on time scales of the same order as the relaxation time of the system $\tau_o = 185$ fs [cf., (8)]. For a period t_p of 2 ps [$\omega = 0.58$ in (65)] the agreement with theory is excellent. This fortunate agreement is due to the fact that the driving force is weak such that the values of $\langle \Delta M \rangle(t)$ are of the same order as the equilibrium fluctuations (7) and the Gaussian description of the distribution underlying (60)−(65) is well-justified. For shorter periods the same description overestimates the simulated hysteresis. For example, for a period of 500 fs ($\omega = 2.32$) one can discern a large overestimation in Figure 8 which may be partially due to the deviation between a monoexponential decay and $C_{M,M}(t)$ which is significant on this time scale, and partially due to errors in the Gaussian description of the equilibrium distribution of $\langle \Delta M \rangle(t)$ (Figure 1) which are pronounced over the 0.3 e Å range probed by the present simulation. For even shorter periods, e.g., for a period of 100 fs ($\omega = 11.6$) presented in Figure 1, the hysteresis is small such that errors in the predictions appear less significant.

Other periodic forms for the periodic field $E(t)$ may be treated similarly, i.e., through integration of (64). We have determined the (piecewise) analytic solution of (64) for the case of the sawtooth potential assumed in the simulation underlying Figure 9 and presented it in this figure. One can recognize that this description underestimates the hysteresis significantly. This deficiency stems from the fact that the relaxation time τ_0, given by (8), is much smaller than the period of 20 ps of the field applied. As pointed out above, the slow dielectric relaxation process apparent in Figure 4 can explain the large hysteresis simulated. Additionally, this simulation explores a range of $\langle \Delta M \rangle(t)$ much larger than that for which the assumption of a Gaussian form for the equilibrium distribution can be supported.

The actual dipole response of a protein is due to a large number of small conformational changes which combine additively to produce the measured response. On the level of single residues a harmonic potential as in the model above would yield much shorter relaxation times than the period of 2 ps presently considered. Therefore, we surmise that the processes underlying the observed hysteresis involve barrier crossings which should be modeled as a random process in ΔM space with the underlying potential $U(\Delta M)$ being a corrugated rather than smooth harmonic potential. This could be treated as a smooth potential with an effective diffusion coefficient determined by the temperature of the system and the roughness of the surface as suggested in ref 46.

If, however, the underlying processes involve barriers with passage times on the order of the driving frequency, then these must be modeled explicitly. To understand the effect of such barriers on the hysteresis loop, we turn to an extreme model in which all of the underlying processes are identical. We can then treat the system as an ensemble where the measured collective dipole response is (proportional to) the mean of the distribution of individual responses.

Figure 16 illustrates the asymptotic behavior of a distribution in a driven bistable potential of the form

$$u(x,t) = \frac{1}{4}x^4 - \frac{1}{2}x^2 - \frac{1}{2}x \sin(\Omega t) \qquad (66)$$

where the coefficient of the driving term is chosen as $^1/_2$ to ensure that the distribution is dumped over the barrier during the cycle. Since an analytical solution for this potential is unavailable, we turn to numerical integration to analyze the behavior of the system following ref 47. By introducing

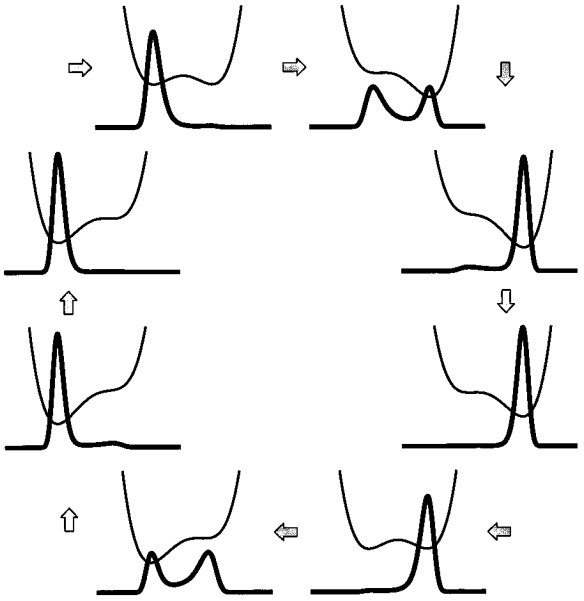

Figure 16. Hysteretic behavior of the distribution in a bistable potential over a full cycle of the applied periodic force: thin line, potential $u(x,t)$; thick line, "steady-state" probability distribution $p(x,t)$ for $\omega = 0.1$, $\beta = 10$. The plot in the upper left corner corresponds to $t = 0$.

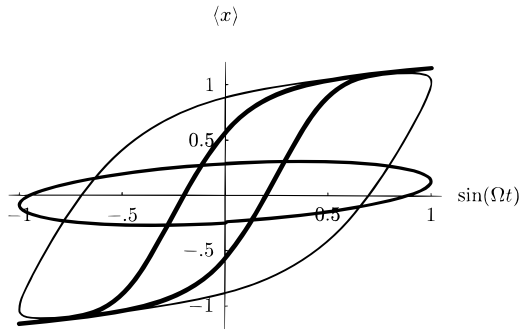

Figure 17. Hysteresis loops for the bistable potential (66) at high, moderate, and low driving frequencies in the dimensionless parameters $\beta \propto 1/k_bT$ and $\omega \propto \Omega$: medium line, high-frequency loop ($\omega = 1$); thin line, moderate-frequency loop ($\omega = 0.1$); thick line, low-frequency loop ($\omega = 0.01$). For these examples, $\beta = 10$. Note that time is in the counterclockwise direction.

appropriate unitless quantities, we can express (61) for a general potential

$$\omega\, \partial_{\Omega t} p(x,t) = \partial_x \left(\frac{1}{\beta}\, \partial_x + \frac{\partial u(x,t)}{\partial x} \right) p(x,t) \qquad (67)$$

for any fixed form of the potential with only the two parameters $\beta \propto 1/k_bT$ and $\omega \propto \Omega$ (see ref 48 for a general discussion), thus making a characterization of the parameter space feasible. Roughly, ω is the driving frequency relative to the local relaxation time of the system, and β is the barrier height relative to the temperature of the system.

We can now make some general observations about the behavior of the driven bistable system. Since the (scaled) barrier height is $^1/_4$, if $1/\beta$ is of this order or larger, the barrier hopping time will be on the same scale as the local relaxation time and the hysteretic behavior of the system will differ little from the harmonic case shown in Figure 15. For smaller temperatures (we selected $\beta = 10$ for the examples) we need to examine three ranges of ω, examples of which are shown in Figure 17.

At very high frequencies the system will have insufficient time to dump between wells during a cycle, and, therefore, local relaxation will again be the primary contribution to hysteresis.

At frequencies which are comparable to the barrier hopping rate, the system will maintain a near-Boltzman distribution during the cycle as adiabatic behavior is observed. Asymptotic approximations for these extremes are found in ref 48. At moderate frequencies we find the region of large hysteresis (as in Figure 16) in which the driving is too fast for the system to hop over the barrier but slow enough for the system to dump between wells when the central barrier is lowered.

Comparison of Figure 15 and Figure 17 demonstrates that larger hysteresis is encountered in a barrier-crossing process than in a simple Ornstein−Uhlenbeck process. This is due to the fact that in the absence of thermal excitation a driven bistable potential will experience hysteresis even in the adiabatic limit, while a simple harmonic potential will not. We therefore conclude that the hysteresis found in our simulations of BPTI which exceeds that predicted by the Ornstein−Uhlenbeck model may be attributed to underlying barrier-crossing events in the protein.

V. Discussion

Our simulations show that, under the influence of an electric field of 10^8 V/m, BPTI does not experience significant changes in either its overall structure or temperature. Stronger fields produce small reversible structural changes within 1 ps but, after application of the field for 2 ps or longer, generate structural changes which relax on a time scale longer than 100 ps. The dipole moment change ΔM due to a weak field, e.g., 10^8 V/m, is so small that it does not even exceed thermal fluctuations. To determine the corresponding dipole moments, we compared the field-off and field-on dynamics of BPTI starting trajectories from identical initial coordinates and velocities. This procedure reduces fluctuations in ΔM substantially for times up to 2 ps. To obtain meaningful results for weak fields, extensive calculations, i.e., large samples, are still needed. Strong fields, on the other hand, show dipole moment changes larger than thermal fluctuations and, hence, require less sampling. Even though such fields are unrealistic or at least difficult to apply experimentally, in an analysis they can shed light on the dielectric properties of proteins.

We employed the relationship between the electric polarization and the external field to evaluate the average dielectric constant, considering the protein as a homogeneous and isotropic dielectric medium. The suggested calculations provide a simple and direct measurement of protein dielectric properties as an alternative to an analysis of dipole fluctuations. The calculated dielectric constant, i.e., 2.62, actually falls into the range of observed values, which is 2−4 [11−13] for dry protein powders. Of course, our calculation included neither bound waters in the protein powder nor electronic polarization. These effects can raise the dielectric constant a little but are not expected to substantially change the dielectric constant of 2.62 beyond the range of 2−4 of the observed values.

We consider the results on dipolar hysteresis presented in this paper of particular importance. Hysteretic behavior is tied to dissipative processes which are likely to occur in nonequilibrium reactions which are common in biological systems. Conventional simulations and models strive for the ideal of quasi-equilibrium and evaluation of thermodynamics potentials. In doing so some relevant features of protein dynamics might remain hidden. For example, our theoretical analysis indicates that dipolar hysteresis reflects the properties of the energy landscape of proteins with its hierarchy of barrier heights. Barriers with crossing times shorter than the period of the applied field can be accounted for through expression (65), whereas barriers with longer crossing times need to be explicitly modeled as done here for a bistable situation. The cardinal role of electrostatic interactions in proteins which couple many, if not nearly all, elementary reaction processes to motions of the protein matrix attribute a key role to dipolar relaxation and dissipation processes.[17,24] However, the treatment of hysteresis in this study might even be of wider relevance since it can be applied to any reaction process.

We have demonstrated that a brief field pulse can induce a complex dipolar response in a protein, in particular, can contribute a dipole echo. For the dipole echo to arise, a significant difference between the frequencies $\tilde{\omega}_\alpha$ and ω_α, i.e., a significant difference of the vibrational frequencies in the presence and absence of an applied field, is required. Such differences are actually consistent with results shown in Figure 6.

The dipole echo effect might be observable through subpicosecond spectroscopy. In femtosecond to picosecond spectroscopy, pump and probe beams are very short so that dipole echo effects should be taken into account. For example, the oscillation of the retinal chromophore in bacteriorhodopsin, observed through light-induced differential transmittance measurements,[49] might originate from a dipole echo response of the protein to short perturbations of pump and probe beams.

Rapid charge shifts could also induce a dipole echo response in proteins. A point charge of one electron generates, over a distance of 10.5 Å, an electric field of 1.31×10^9 V/m, which can induce a significant echo effect as demonstrated in Figure 11. This suggests that dipole echoes may arise in proteins for fast redox reactions. We have suggested also in ref 27 that a dipole echo is involved in the so-called *J* intermediate of the proton pump cycle of bacteriorhodopsin, which exhibits a spectral transition after rapid photoisomerization that cannot be thermally stabilized.

There exist other systems which invite respective studies. One example is the photosynthetic reaction center which exhibits oscillations with a period of 400 fs to 2 ps during stimulated emission and absorption.[50,51] The authors in refs 50 and 51 suggest that the oscillations are due to protein modes which are strongly coupled to photoinduced electron transfer. Oscillations are also observed during the first few picoseconds of the decay in the spontaneous fluorescence of the special pair in bacterial photosynthetic reaction centers.[52] In this respect it is of interest that a simulation of the energy gap correlation function which (in linear response theory as shown in ref 19) describes the response of the protein matrix to electron transfer exhibits oscillations with a period of 500 fs.[20]

The methodology introduced here may be applied to describe dielectric responses of proteins to local fields or to inhomogenous fields as they arise for proteins in water. We considered here the case of homogenous external fields, since such fields are well-defined and since the dipolar response to such field can be derived analytically. In the case of proteins in water, studied for example in refs 8, 10, and 53, gradients of electrostatic potentials generated experimentally are not homogenous, e.g., are larger inside the protein. It appears to be desirable to extend the study here to investigate the combined protein/solvent response in the presence of time-varying electrostatic fields.

We note finally that we have focussed our investigation mainly on BPTI at low temperature, namely, $T_0 = 100$ K. The reason for this choice is the relatively small size of thermal fluctuations of $\Delta M(t)$ which allowed small sample sizes. However, BPTI at physiological temperatures might exhibit a qualitatively different pattern of dipolar relaxation than determined in this article, i.e., may not exhibit significant hysteresis

for cyclic fields. However, now that the methodological aspects for the simulation of dipolar relaxation properties have been established, it is a straightforward task (see Figure 5) to extend investigations to physiological temperatures.

Acknowledgment. The authors thank M. Fixman for a critical reading of an earlier version of this paper and A. Warshel for helpful comments. The research was carried out at the Resource for Concurrent Biological Computing at the University of Illinois, funded by the National Institutes of Health (Grant P41RR05969), by the the National Science Foundation (Grants BIR-9318159 and ASC-8902829), and by the Roy J. Carver Charitable Trust. J.C.P. has been supported by the U.S. Department of Energy Computational Science Graduate Fellowship Program.

References and Notes

(1) Grant, E. H.; Sheppard, R. J.; South, G. P. *Dielectric Behaviour of Biological Macromolecules in Solution*; Clarendon Press: Oxford, U.K., 1978.
(2) Demchenko, A. P. *J. Mol. Liq.* **1993**, *56*, 127.
(3) Smith, P. E.; Brunne, R. M.; Mark, A. E.; van Gunsteren, W. F. v. *J. Phys. Chem.* **1993**, *97*, 2009.
(4) Simonson, T.; Perahia, D.; Bricogne, G. *J. Mol. Biol.* **1991**, *218*, 859.
(5) Simonson, T.; Perahia, D. *Proc. Natl. Acad. Sci. U.S.A.* **1995**, *92*, 1082.
(6) Warshel, A.; Russell, S. T. *Q. Rev. Biophys.* **1984**, *17*, 283.
(7) Honig, B.; Nicholls, A. *Science* **1995**, *258*, 1144.
(8) King, G.; Lee, F.; Warshel, A. *J. Chem. Phys.* **1991**, *95*, 4366.
(9) Warshel, A.; Aqvist, J. *Annu. Rev. Biophys. Biophys. Chem.* **1991**, *20*, 267.
(10) Niedermeier, C.; Schulten, K. *Mol. Simul.* **1992**, *8*, 361.
(11) Takashima, S.; Schwan, H. P. *J. Phys. Chem.* **1965**, *69*, 4176.
(12) Pennock, B. D.; Schwan, H. P. *J. Phys. Chem.* **1969**, *73*, 2600.
(13) Harvey, S. C.; Hoekstra, P. *J. Phys. Chem.* **1972**, *76*, 2987.
(14) Bone, S.; Pethig, R. *J. Mol. Biol.* **1985**, *181*, 323.
(15) Deisenhofer, J.; Steigemann, W. *Acta Crystallogr. B* **1975**, *31*, 238.
(16) Steffen, M. A.; Lao, K. Q.; Boxer, S. G. *Science* **1994**, *264*, 810.
(17) Schulten, K. Curve crossing in a protein: Coupling of the elementary quantum process to motions of the protein. In *Proceedings of the Ecole de Physique des Houches*, 85, Paris, 1995; Bicout, D., Field, M. J., Eds.; Les Editions de Physique; Springer: Berlin, 1995.
(18) Treutlein, H.; Schulten, K.; Brünger, A.; Karplus, M.; Deisenhofer, J.; Michel, H. *Proc. Natl. Acad. Sci. U.S.A.* **1992**, *89*, 75.
(19) Nonella, M.; Schulten, K. *J. Phys. Chem.* **1991**, *95*, 2059.
(20) Schulten, K.; Tesch, M. *Chem. Phys.* **1991**, *158*, 421.
(21) Warshel, A.; Chu, Z. T.; Parson, W. W. *Science* **1989**, *246*, 112.
(22) Warshel, A.; Parson, W. W. *Annu. Rev. Phys. Chem.* **1991**, *42*, 279.
(23) Xu, D.; Schulten, K. Multi-mode coupling of protein motion to electron transfer in the photosynthetic reaction center: Spin-boson theory based on a classical molecular dynamics simulation. In *The Photosynthetic Bacterial Reaction Center: II. Structure, Spectroscopy and Dynamics*; Breton, J., Vermeglio, A., Eds.; NATO ASI Series A: Life Sciences, 301; Plenum Press: New York, 1992.
(24) Xu, D.; Schulten, K. *Chem. Phys.* **1994**, *182*, 91.
(25) Delaney, J. K.; Brack, T. L.; Atkinson, G. H.; Ottolenghi, M.; Steinberg, G.; Sheves, M. *Proc. Natl. Acad. Sci. U.S.A.* **1995**, *92*, 2101.
(26) Du, M.; Fleming, G. R. *Biophys. Chem.* **1993**, *48*, 101.
(27) Xu, D.; Martin, C.; Schulten, K. *Biophys. J.* **1996**, *70*, 453.
(28) Becker, O. M.; Karplus, M. *Phys. Rev. Lett.* **1993**, *70*, 3514.
(29) Xu, D.; Schulten, K.; Becker, O. M.; Karplus, M. *J. Chem. Phys.* **1995**, *103*, 3112.
(30) Xu, D.; Schulten, K. *J. Chem. Phys.* **1995**, *103*, 3124.
(31) Windemuth, A.; Schulten, K. *Mol. Simul.* **1991**, *5*, 353.
(32) Board, J. A., Jr.; Causey, J. W.; Leathrum, J. F., Jr.; Windemuth, A.; Schulten, K. *Chem. Phys. Lett.* **1992**, *198*, 89.
(33) Brooks, B. R.; Bruccoleri, R. E.; Olafson, B. D.; States, D. J.; Swaminathan, S.; Karplus, M. *J. Comput. Chem.* **1983**, *4*, 187.
(34) Connolly, M. L. *J. Appl. Crystallogr.* **1983**, *16*, 548.
(35) Connolly, M. L. *J. Mol. Graphics* **1993**, *11*, 139.
(36) Müller-Plathe, F.; Rogers, S. C.; Gunsteren, W. F. v. *J. Chem. Phys.* **1993**, *98*, 9895.
(37) Kirkwood, J. G. *J. Chem. Phys.* **1939**, *7*, 911.
(38) Fröhlich, H. *Theory of Dielectrics*; Oxford: London, 1958.
(39) Lerner, R. G.; Trigg, G. L. *Encyclopedia of Physics*, 2nd ed.; VCH: New York, 1990.
(40) Schulten, K.; Lu, H.; Bai, L. Probing protein motion through temperature echoes. In *Physics of Biological Systems*; Flyvbjerg, H., Mouritsen, O. G., Eds.; Springer's LNP; Springer: in press.
(41) Wang, M. C.; Uhlenbeck, G. E. *Rev. Mod. Phys.* **1945**, *17*, 323.
(42) Chandrasekhar, S. *Rev. Mod. Phys.* **1943**, *15*, 1.
(43) Wolfram, S. *Mathematica, A System for Doing Mathematics by Computer*, 2nd ed.; Addison-Wesley: New York, 1991.
(44) Schulten, K.; Schulten, Z.; Szabo, A. *Physica* **1980**, *100A*, 599.
(45) Jung, P. *Phys. Rep.* **1993**, *234*, 175.
(46) Nadler, W.; Schulten, K. *Proc. Natl. Acad. Sci. U.S.A.* **1984**, *81*, 5719.
(47) Phillips, J.; Schulten, K. Modeling AFM tip dynamics through diffusion in time-periodic potentials. In *NATO Advanced Research Workshop on Atomic Force Microscopy*; Gaub, H., Ed.; NATO ASI Series B; Plenum Press: New York, in press (Beckman Institute Technical Report TB-95-03).
(48) Phillips, J.; Schulten, K. *Phys. Rev. E* **1995**, *52*, 2473.
(49) Dexheimer, S. L.; Wang, Q.; Peteanu, L. A.; Pollard, W. T.; Mathies, R. A.; Shank, C. V. *Chem. Phys. Lett.* **1992**, *188*, 61.
(50) Vos, M. H.; Lambry, J. C.; Robles, S. J.; Youvan, D. C.; Breton, J.; Martin, J. L. *Proc. Natl. Acad. Sci. U.S.A.* **1992**, *89*, 613.
(51) Vos, M. H.; Rappaport, F.; Lambry, J. C.; Breton, J.; Martin, J. L. *Nature* **1993**, *363*, 320.
(52) Stanley, R. J.; Boxer, S. G. *J. Phys. Chem.* **1995**, *99*, 859.
(53) Honig, B.; Sharp, K.; Yang, A. *J. Phys. Chem.* **1993**, *97*, 1101.

JP960076A